3-2021

Satellite Tracking with Neuromorphic Cameras for Space Domain Awareness

Joseph G. Bacon Jr.

Satellite Tracking with Neuromorphic Cameras for Space Domain Awareness

THESIS

Joseph G. Bacon Jr., Capt, USSF

AFIT-ENY-MS-21-M-286

DEPARTMENT OF THE AIR FORCE
AIR UNIVERSITY

AIR FORCE INSTITUTE OF TECHNOLOGY

Wright-Patterson Air Force Base, Ohio

AFIT-ENY-MS-21-M-286

SATELLITE TRACKING WITH NEUROMORPHIC CAMERAS FOR SPACE DOMAIN AWARENESS

THESIS

Presented to the Faculty

Department of Aeronautics and Astronautics

Graduate School of Engineering and Management

Air Force Institute of Technology

Air University

Air Education and Training Command

in Partial Fulfillment of the Requirements for the

Degree of Master of Science in Space Systems

Joseph G. Bacon Jr., B.S.

Capt, USSF

25 March 2021

AFIT-ENY-MS-21-M-286

SATELLITE TRACKING WITH NEUROMORPHIC CAMERAS FOR SPACE DOMAIN AWARENESS

THESIS

Joseph G. Bacon Jr., B.S.
Capt, USSF

Committee Membership:

Lt. Col. Bryan D. Little, Ph.D.
Chair

Richard G. Cobb, Ph.D.
Committee Member

Andrew S. Keys, Ph.D.
Committee Member

Abstract

A significant number of objects orbit the space around Earth. Each of these objects, be it debris, a functioning satellite, or even a staffed space station, circle the planet at extreme speeds relative to most objects on the Earth's surface. Any collision would result in disaster thanks to the extreme amount of kinetic energy involved. Space Domain Awareness (SDA) includes the detection, identification, cataloging, and tracking of orbiting objects to prevent such catastrophes. SDA is maintained in multiple ways to include radar, lidar, telescopes, and other sensors. This research investigates the maturing technology of neuromorphic cameras to determine their applicability to SDA. The DVS240C camera was integrated with two telescopes to assess its ability to perform astrometric measurements and observations of satellites for orbit updates. The findings show that astrometry was difficult to conduct with this setup and more analysis is needed with different equipment to better assess this style of camera's astrometric capabilities. This research did find that orbit updates are possible and that this technology provides angle rate data not attainable with frame-based CCD cameras.

Acknowledgements

I want to offer my sincere thanks to all who made this research effort possible. First, I want to thank my wife and daughter for all their support and love during this chapter of our lives. It's taken many months to get through this and it would not have been possible without their help and care. Second, I would like to thank Lt Col Bryan Little who provided guidance, imparted his knowledge, and remained patient with me throughout this interesting time at AFIT. COVID-19 really brought some interesting changes and challenges to everyone's lives and without my family and Lt Col Little, none of this would have been possible.

Joseph G. Bacon Jr.

Table of Contents

Page

List of Figures

List of Tables

SATELLITE TRACKING WITH NEUROMORPHIC CAMERAS FOR SPACE DOMAIN AWARENESS

I. Introduction

1.1 Background

Space is becoming more congested and contested as time continues on. More parties are able to attain the necessary technologies to reach space meaning more debris and satellites are having to share the environment, especially when highly important regions of interest, e.g. geosynchronous orbit, are taken into account.[6] As space becomes more crowded, more objects need to be tracked and accounted for, not only to prevent accidental crashes like the Iridium-33 and Kosmos 2251 spacecraft which created thousands more objects after the collision but also to provide safety of flight for future missions.[7] Debris has no ability to maneuver and poses a regular and reoccurring threat to any spacecraft in a close orbit or in an orbit that travels through the debris' path. Keeping track of all resident space objects (RSO) helps ensure the protection of extremely expensive assets which likely cost millions of dollars to produce and send into orbit. If an asset happens to contain any life aboard, the expense would be incalculable as any collisions would almost certainly result in loss of life. Space Domain Awareness (SDA) is the process of data collection and analysis to combat this increasingly insurmountable issue.

Space Domain Awareness (SDA) is defined as "the actionable knowledge required to predict, avoid, deter, operate through, recover from, and/or attribute cause to the loss and/or degradation of space capabilities and services."[6] One part of SDA

is Space Situational Awareness defined as "the perception of the elements in the environment within a volume of time and space, the (organizational) comprehension of their meaning, and the projections of their status in the near future."[8] Even inactive objects or debris which have no means of altering their orbit must regularly be tracked for the reasons stated previously. While a basic orbit can be approximated using two-body orbital mechanics, reality is much more complicated. There are a number of perturbations which influence an object's orbit, e.g. atmospheric drag, solar pressure, uneven distribution of Earth's mass and aspherical shape, the multi-body problem. If an object in space is not regularly tracked and accounted for and its orbit path updated, it will be lost because of these factors that alter its orbit. If an object is lost, it cannot be accounted for and thus there is no way to prevent a collision. There are several methods available to track an object in space.

Telescopes and optical observation of satellites to this day remains pertinent to maintaining Space Domain Awareness (SDA). Other methods of SDA upkeep have significant drawbacks. For example, radar suffers significant power loss due to distance, by a factor of $1/r^4$, but generally is not affected by weather conditions. In general, lidar and optical methods are weather dependent and suffer from a reduction in capability when wind, clouds, or rain are involved in the optical path. Lidar has the potential to damage sensors on satellites if not precisely controlled, ruining expensive equipment. Other optical methods such as telescopes are becoming more available and cheaper making them increasingly more attractive for maintaining SDA.[6]

Current optical systems for SDA use Charge Coupled Device (CCD) or Complementary Metal Oxide Semiconductor (CMOS) cameras that operate in a somewhat limited capacity. These camera types open their shutter to allow light to collect on pixels which convert the light collected into a digital report of intensity for various wavelengths which is converted into a standard image. To record meaningful informa-

tion for SDA, these cameras will open their shutter for some predetermined exposure time to collect enough light to show the path satellites travel. If they open and close too quickly, not enough data will be collected to understand the satellites current orbit and predict its future position with an orbit update. If the shutter is open too long, the pixel array could become over-saturated and the image produced would be washed out and unusable for orbit updates. These camera styles also suffer from large data outputs as a result of every pixel being used for each frame generation. This research explores a different style of camera for SDA which does not suffer from the same drawbacks.

In the 1990s, a new style of camera was developed called Neuromorphic cameras, also known as event-based cameras, which operate in an entirely different manner from the standard digital camera. This technology does not collect light and report intensity in the same way CCD and CMOS sensors do but instead, each pixel reports changes in intensity asynchronously and is thus not limited in the same capacity as a standard camera. These cameras are adept at tracking movement and do not suffer from the same over-saturation issues. They also have a smaller data output as only the triggered pixels output event data.[1, 2, 9, 10, 11] This leads to various research questions about how they could be used for SDA.

1.2 Research Objectives

This research explores how neuromorphic sensors might be utilized for SDA. The following research questions and associated tasks were investigated:

1. What type of information can be discerned with a neuromorphic camera observing satellite passes and under what conditions can they be observed?
    (a) Determine azimuth and elevation look angles for objects in view.
    (b) Determine rate of change of azimuth and elevation look angles.

2. How well can you perform orbit updates for observed objects with a neuromorphic sensor using pixel location and telescope mount angle?

   (a) Use the collected data from observation with a staring telescope to perform a sequential update.

3. Can astrometry be performed on neuromorphic derived imagery?

   (a) Perform an astrometric determination of pointing direction based upon observed stars.

   (b) Use determined pointing direction and astrometry to calculate a more accurate track of an object's pass.

1.2.1 Assumptions and Limitations

The scope of this research is limited to using a DVS240C neuromorphic camera with a telescope set up in a stationary staring orientation to observe objects passing overhead The camera is operated via Inivation's DV software designed for the camera. The software code developed for data type conversion and analysis is limited to Python and MATLAB. Equipment is limited to what is currently available within the AFIT ENY department. One of the main expected challenges will be acquiring enough stars in view to perform astrometry.

This research proceeds under a few assumptions. First, that the telescopes utilized will be able to capture enough stars for astrometry. Some other assumptions include that the telescope locations are assumed to be known accurately. Once an observation is recorded, it is assumed that Two-Body Propogation (2BP) methods can be used to generate state estimates at the time of observation from an initial TLE state. Additionally, covariances are assumed to be normally distributed.

If all the research objectives are reached, neuromorphic cameras will be shown

as an excellent, if not superior, method of maintaining SDA when compared against frame-based cameras. It is expected that these cameras will eventually be incorporated on an operational scale and could potentially be automated to constantly improve SDA.

1.3 Thesis Outline

This research is comprised of five parts: The introduction, the background and literature review, the methodology used for research, the analysis of collected data, and the conclusions drawn from experimentation. Chapter II, the background and literature review, further explains the technology of neuromorphic cameras, what has been done before with event-based cameras relative to SDA, and an explanation of astrometry and its uses. Chapter III describes the equipment and setup used for experimentation, their capabilities and limitations, and the type of data gathered. Chapter IV analyzes the data collected from the equipment used. Chapter V concludes the document by summarizing the essential findings from analysis and how these cameras can be used for SDA and may be a better alternative to other SDA capabilities.

II. Literature Review

2.1 Background and Related Theory

This chapter provides an overview of topics and theory related to the research conducted. First, neuromorphic cameras are introduced with an overview of their operation. Second, an overview of telescopes and how they are used to collect RSO observations is explained. Third, a brief explanation of astrometry is provided. Finally, an explanation on astrodynamics, specifically how uncertainty influences our understanding of an object's orbit and why we need to re-observe objects for SDA as well as different methods for updating object orbits.

2.1.1 Neuromorphic Cameras

Neuromorphic cameras, also known as event-based cameras, are a type of optical technology that was originally developed in the 1990s. These cameras were developed in an effort to mimic more accurately the biological eye which is very much suited for tracking movement and changes in the environment rather than measuring light intensity and creating still images.[9] Event-based cameras do not operate with a shutter. Instead, the pixel array triggers when the log intensity of measured light changes by a predetermined amount which generates a recorded event. The typical pixel schematic for the Dynamic Vision Sensor (DVS) version of these cameras is shown in Figure 1 [1]

In Figure 1, the photoreceptor outputs a logarithmic intensity which the differencer compares against the last event to detect changes. The pixel reports an ON or OFF event when the intensity breaches a threshold amount set by the comparators. Each pixel reports a trigger, or "event", asynchronously rather than output an image or series of images at a time.

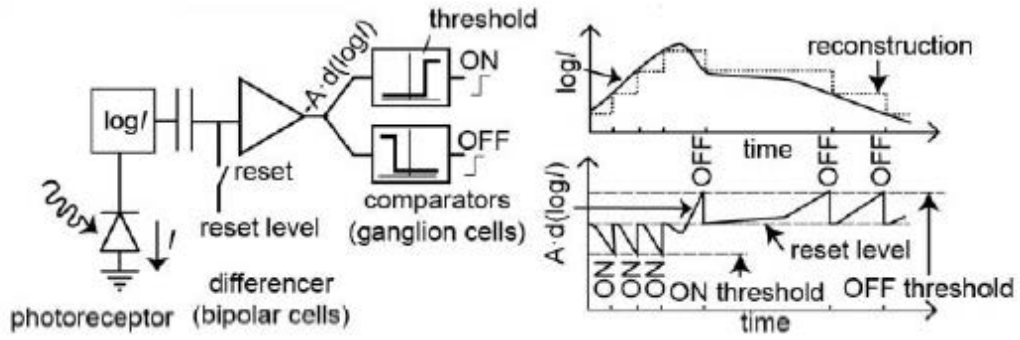

Figure 1. DVS Simplified Pixel Schematic (Delbruck, 2016)[1]

Neuromorphic cameras output a stream of "events" which are organized as such:

$$e = [x, y, p, t] \tag{1}$$

where e is the event reported, x and y are the pixel coordinates for the event, p represents polarity and is either a one or zero designating an increase or decrease respectively in light intensity measured, and t represents the time at which the event is generated by the camera in milliseconds.[12] Figure 2 provides a visual depiction of events recorded from a neuromorphic camera observing a rotating black bar.[2] Figure 2 is a depiction of the event generation meant to help comprehension but typically, the result is displayed on a user interface that looks similar to Figure 3. In Figure 3, Jupiter was recorded using a telescope and the DVS240C event-based camera. Each lit pixel is a recorded event where green denotes an increase in intensity measured while red represents a decrease. In this case, Jupiter was shifting towards the right of the camera's field of view.

The unique operation of these cameras provides them several advantages besides the lack of over-saturation. The asynchronous pixel operation provides a very high temporal resolution. They also operate with a high dynamic range and have low power

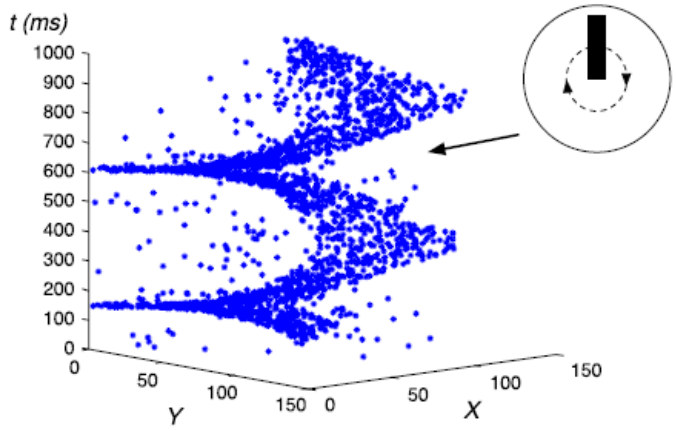

Figure 2. Visualization of recorded events for a rotating black bar (Benosman, 2012)[2]

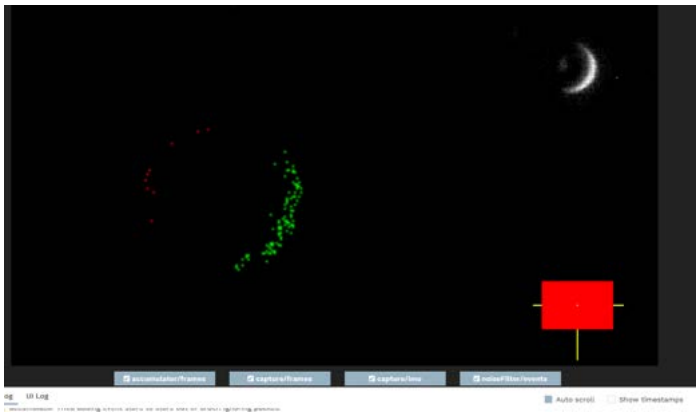

Figure 3. Screenshot of recording Jupiter with the DVS240C and DV software.

consumption as well as reduced bandwidth requirements.[2, 11] The development of these cameras has led to a need to redefine image processing, signal processing and algorithm development.

Recent work has attempted to study how these cameras might be applicable to SDA, specifically, previous research has shown that these cameras can be used for generating star maps to use with conventional astrometry software [12], and have been compared to frame-based cameras for object detection and tracking [11]. What has not been reported yet is if these cameras can record satellite movement to perform orbit updates. One method of acquiring the data needed for an update is by using

the sensor with a telescope.

2.1.2 Telescopes

Telescopes operate by using lenses or mirrors to bend and focus light onto a sensor, e.g. photographic plate, CCD, etc. There are three basic types of telescopes: refracting, reflecting, and catadioptric as shown in Figure 4. Additional variations exist but are considered variations of the main three types. Refracting telescopes use lenses to focus light, reflecting telescopes use mirrors, and catadioptric, also known as complex, use both lenses and mirrors to direct light. The focal length of the

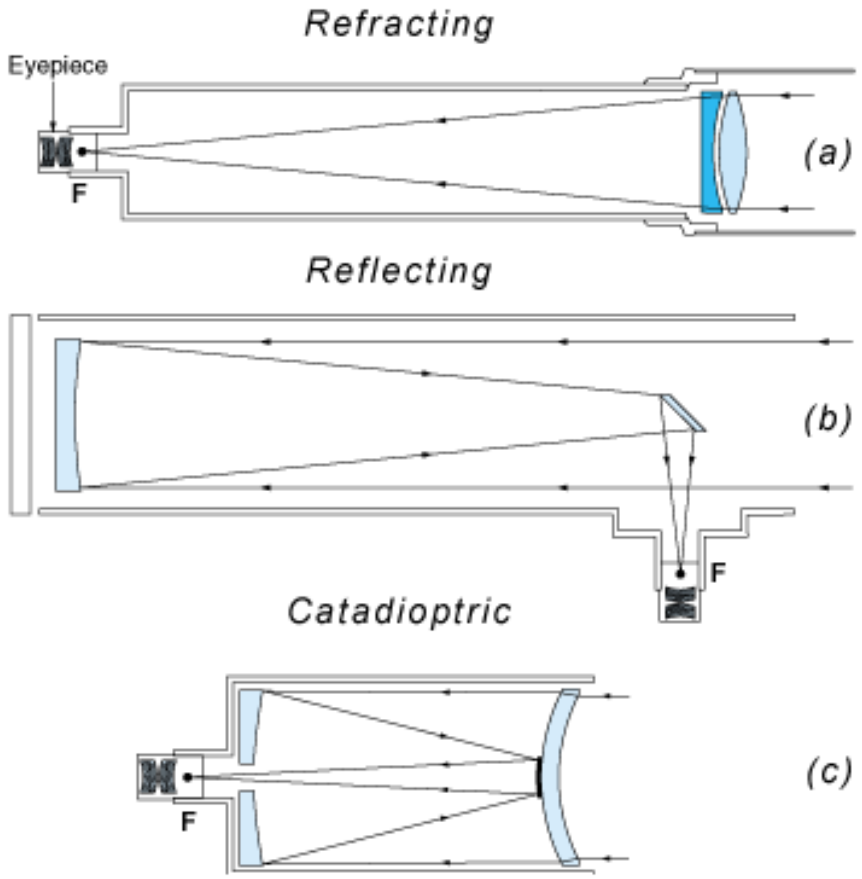

Figure 4. Three Basic Types of Telescopes (Meade Instruments Corporation)[3]

telescope, determined by the internal setup of lenses, mirrors, etc., is the main factor

that determines how much an object is magnified. When a telescope is used to observe satellites, it is typically oriented using azimuth and elevation to describe where the telescope is pointing. Azimuth describes the angular distance from either the North or South direction while elevation describes the vertical angular distance from the horizon. These directions are defined in a local, also known as a topocentric, coordinate frame. Figure 5 visually demonstrates this coordinate frame. Using this

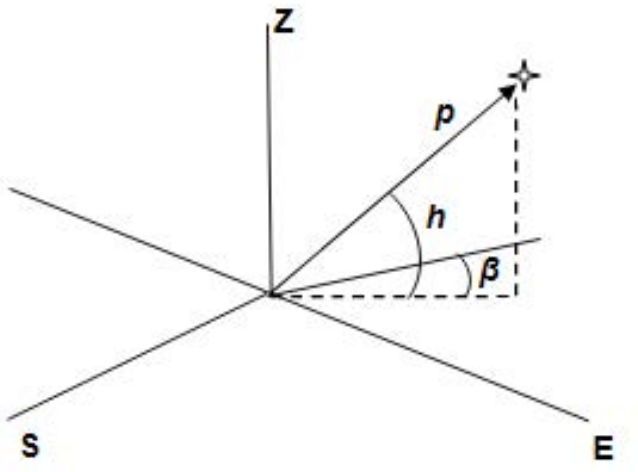

Figure 5. Topocentric Coordinate Frame (Wiesel, 2003)[4]

coordinate frame, an observed object's position can then be described relative to the telescope. In order to use the telescope's measurement for orbital updates later, that measurement frame must be rotated to the Earth-Centered Inertial (ECI) frame by Direction Cosine Matrices, also known as rotation matrix.[13] Equation 2 calculates the position of the telescope in the geocentric reference frame which is the origin for Figure 5.

$$\vec{r}_{st} = r * \begin{bmatrix} \cos(lat) * \cos(lon) \\ \cos(lat) * \sin(lon) \\ \sin(lat) \end{bmatrix} \tag{2}$$

$\vec{r}_{st}$ is the radius from center of earth to the telescope while "lat" and "lon" are the latitude and longitude of the telescope's location.

Measurements taken with a telescope are not perfect. Many factors influence and distort the observation made. For example, atmospheric diffraction, optical aberrations, errors in measurement for telescope pointing, and even how the collected light lands on the pixel array and is generally spread over multiple pixels making the true center indeterminable, all interfere with measurement accuracy. The more of these measurement errors that are included in an orbit estimate and are corrected for, the more accurate the result.[4, 13]

2.1.3 Astrometry

Astrometry is the use of stars and their known positions to accurately assess where a telescope is pointing and the location of other objects within view based upon star geometry. Figure 6 depicts an optical sensor, set at the origin, viewing a star field in the top right with its pixel array in the bottom left. As light from the stars enters the sensor through the origin, it reaches the pixels where the camera creates an image based upon the light gathered. When stars are observed by a sensor, those stars can be compared against a star catalog to determine which stars are in view. Then, the known positions of the stars geometry can be used to determine the center of the FOV, represented by α_0 and δ_0 in 6, the right ascension and declination of the sensor. Once the center of the FOV is known, then the position of another object that was previously unknown can be calculated based upon pixel location relative to the center of the FOV. Using the pointing knowledge and pixel location of where light collected for an object of interest, the right ascension and declination, α and δ, of the object

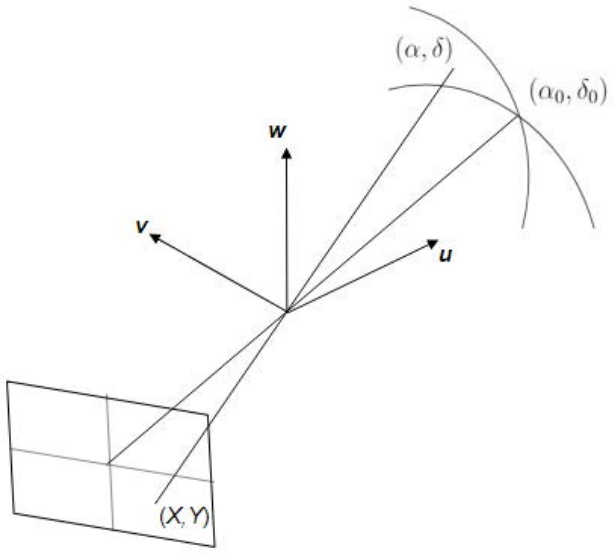

Figure 6. Photographing a Starfield (Montenbruck, 2003)[5]

can be determined using Equations 3 and 4.[5]

$$\alpha = \alpha_0 + \arctan\left(\frac{-X}{\cos(\delta_0) - Y\sin(\delta_0)}\right) \tag{3}$$

$$\delta = \arcsin\left(\frac{\sin(\delta_0) + Y\cos(\delta_0)}{\sqrt{1 + X^2 + Y^2}}\right) \tag{4}$$

Various tools such as astrometry.net are available that allow a user to input an astronomical image of the sky and if enough stars are visible within the image, the tool will return the astrometric calibration data, which includes the center of the FOV, along with the list of known objects within view.[14] This provides a relatively easy way to determine the center FOV of an image to begin performing astrometric calculations, provided enough stars are in view.

2.2 Astrodynamics

2.2.1 Uncertainty and the Need to Maintain SDA

In general, Equation (5) is the Two-Body Problem Equation of Motion that introduces additional acceleration acting on an object in Keplerian motion.[13]

$$\ddot{\vec{r}} = -\frac{\mu}{r^3}\vec{r} + \vec{a}_d \tag{5}$$

Where $\ddot{\vec{r}}$ is the acceleration of the object, μ is the gravitational parameter, r is the position of the object, and $\vec{a_d}$ is an external acceleration acting upon the object.

Several factors can influence an object's motion in space. For example, the Earth is aspherical meaning that different areas of the planet exhibit different gravitational forces. Atmospheric drag also influences the motion of an object stronger the closer the object is to the Earth. Another example is the gravitational effects of other bodies in space or solar radiation pressure acting on an object. All these factors make it difficult to accurately, and impossible to perfectly, describe an orbiting object's motion which creates uncertainty in position and velocity. Over time, that uncertainty will grow. One method of trying to account for that uncertainty is by using what is called the covariance. Covariance is a way to mathematically describe the unknowns involved.[4] When used for describing an object's orbit, the covariance represents a ellipsoid of possibility where the object could actually be located as shown in Figure 7. Over time, that covariance, or uncertainty, will grow meaning we are less confident in the exact known location of the object. This creates an issue for SDA so regular observations and updates of orbiting objects must be taken to reduce the covariance.

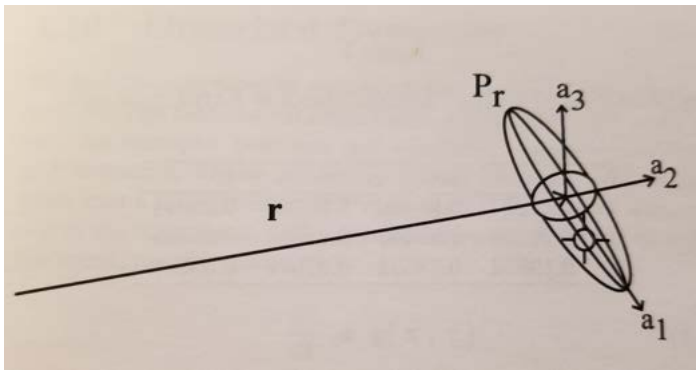

Figure 7. Predicted Position and Covariance Ellipsoid, (Wiesel, 2003)[4]

2.2.2 Orbit Updates from Earth Observations

All orbits described using orbital dynamics are just estimations of the observed dynamic state of the orbiting object. Due to the numerous forces, both natural and artificially occurring, on an orbiting object, that estimated dynamic state rapidly deteriorates when not continuously observed and updated. What may have started as Kepler's Problem, predicting the future state of a satellite in orbit has been studied vigorously.[13] Today, with the help of the modern computer and tools like Differential Correction, Batch Least Squares, and Kalman's estimation theory, uncertainty is incorporated into maintaining SDA.[4]

In addition to accounting for uncertainty, the sheer number of RSOs compared to the number of available sensors is staggering. Adding to that problem, each sensor can only see and track a limited number of objects due to the observable FOV. In addition to increasing the number of sensors, tasking sensors needs to be optimized. This has been studied in other research efforts leading at first to survey and follow-up methods where a telescope observes a target, a future position is predicted, and the telescope is pointed to the new expected position where a follow-up observation and update is attempted. Other tasking strategies have since been developed such as cost function models to evaluate sensor tasking scenarios, combining finite set statistics

with sensor tasking, and even an optimization problem that uses a weighted sky area approach in combination with a diversification of the optimization scheme.[15, 16, 17] While still critical to SDA, this research focuses more on a new technology to use for observations rather than tasking optimization.

As newer technologies are developed, additional opportunities arise to further improve SDA. One research effort has shown that commercial telescopes can be used for initial determination of low earth orbits, showing that large scale expensive telescopes are not needed to make an orbit determination.[18] Another research effort has built upon that by developing modularized software architecture to further improve SDA.[19] Neuromorphic cameras have even been comparatively evaluated against frame-based cameras in terms of detection and tracking capabilities. While not shown to be suitable to replace frame-based technology, it has been shown that there is significant value in researching this technology further.[11]

2.3 Summary

Chapter II detailed some required information to better understand how to answer the research questions previously posed in Chapter I. Neuromorphic cameras and their operation, telescopes and how they can measure information on an object, an into to astrometry, and finally some astrodynamic impacts were explained. Armed with this knowledge, the methodology explained in the next chapter is more easily understood.

III. Methodology

3.1 Research Methodology

3.1.1 Introduction

This chapter discusses the methodology and techniques used during research to observe satellites and collect data. First, the telescope setups are explained which outline the hardware used. Next, the observations recorded are detailed. Finally, the methodology for processing and analyzing the data is described where the approximate telescope azimuth and elevation is used via the Kalman filter update equations to update the object's predicted orbit.

3.1.2 Equipment Setups

During this research effort, two different setups were used to observe satellites. Each setup used a different telescope. The first used a Meade 10-inch and the second a Takahashi 106mm.[20, 21] Each was equipped with one type of neuromorphic camera, the DVS240C and a 0.5 optical reducer to increase the Field of View (FOV). The Takahashi telescope was mounted on an Astro-Physics 1100 GTO servo drive while the Meade telescope has its own built in mount and drive. Initially, each telescope was used independently for observations with the exception being the final observation where both telescopes were setup next to each other. The Takahashi was equipped with the camera while the Meade was used to estimate azimuth and elevation. The two telescopes are shown in Figure 8. Only one telescope was equipped with the camera at a time. The DVS240C camera, shown in Figure 9 is a neuromorphic camera developed by iniVation. The pixel array is 240 by 180 pixels that are 18.5 micrometers square on an array size of 4.44 by 3.33 millimeters. The dynamic range is 130dB and the power consumption of the camera is less than 180mA at 5V DC.

Figure 8. Takahashi 106mm with DVS240C camera and optical reducer on the left with the Meade 10-inch (no sensor attached) on the right.

Figure 9. DVS240C Neuromorphic Camera Front

The approximate FOV for each setup was calculated using the following formula:

$$FOV = \frac{D}{f} * \frac{180}{\pi} \tag{6}$$

where FOV is the degrees visible in the FOV, D is the relative dimension size of the pixel array and f is the telescope's focal length. The list of equipment for each setup and their characteristics are listed in Table 1.

Table 1. Telescope Equipment and Attributes with DVS240

Telescope	Focal Length (mm) w/reducer	FOV (deg hor x ver)
Takahashi 106mm	265	0.96 x 0.72
Meade 10-Inch	1270	0.2 x 0.15

Heavens-above.com was used to predetermine satellite observations for optimal chance of success.[22] Satellite passes were prioritized by brightness and relative proximity to the highest number of stars based upon sky charts depicting orbit path, timing, and brightness data provided by heavens-above.com. Each telescope was manually pointed to areas of interest in the sky using constellations and stars known to be close to or on the direct orbit path. The Meade telescope mount was used to measure azimuth and elevation. The DVS240C camera was operated via Inivation's DV software running on a laptop and connected via USB.[23] Focus was manually adjusted to ensure stars in view were as small as possible. As expected observation time approached, the camera was set to record. Typically, small adjustments to the telescope pointing were needed as the earth rotated and forced stars out of the camera's FOV.

3.1.3 Observations

Five observations were recorded over a three month period of experimentation and research. Table 2 below lists each object observed, the time and date of observation, and the telescope used for observation. These observations were chosen based upon relative brightness data and proximity to stars discerned from heavens-above.com. To record data, the camera was connected via USB to a laptop running iniVation's DV software which recorded events into a .aedat4 file. The Address Event Data (AEDAT)

file format is a custom data type created by iniVation which stores the pixel location, polarity, and time event data. For the first observation, the Chang Zheng-4 (CZ-4

Table 2. Observation Objects, Time and Date, and Telescope Setup

Object	Observation Time, Date	Telescope Setup Used
Chang Zheng-4 Rocket body (CZ-4 R/B)	1853, 04 Nov 2020	Meade 10-Inch
Sich 1	1859, 19 Nov 2020	Takahashi 106mm
Cosmos 2237	1807, 23 Nov 2020	Takahashi 106mm
Starlink 1066	1812, 2 Dec 2020	Takahashi 106mm
Yaogan-1	1845, 10 Jan 2021	Takahashi 106mm with sensor Meade for Az/El estimate

R/B) Rocket Body was observed passing through the constellation Andromeda, next to the star Mirach. Figure 10 below is a sky chart from Heavens-Above.com which depicts the object's predicted orbital path. Figure 11 below is zoomed in on the same

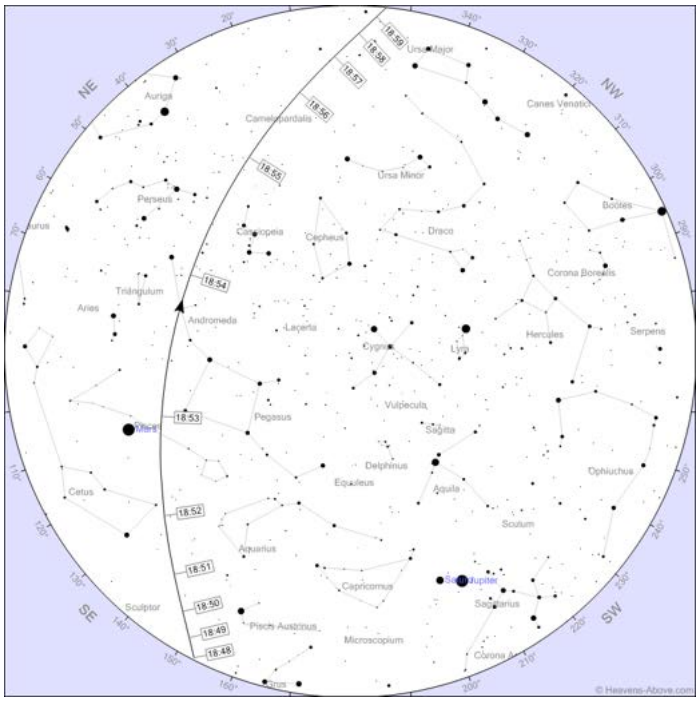

Figure 10. Heavens-Above.com image of CZ-4 R/B overhead pass

sky chart with the approximate FOV of the recorded event outlined.

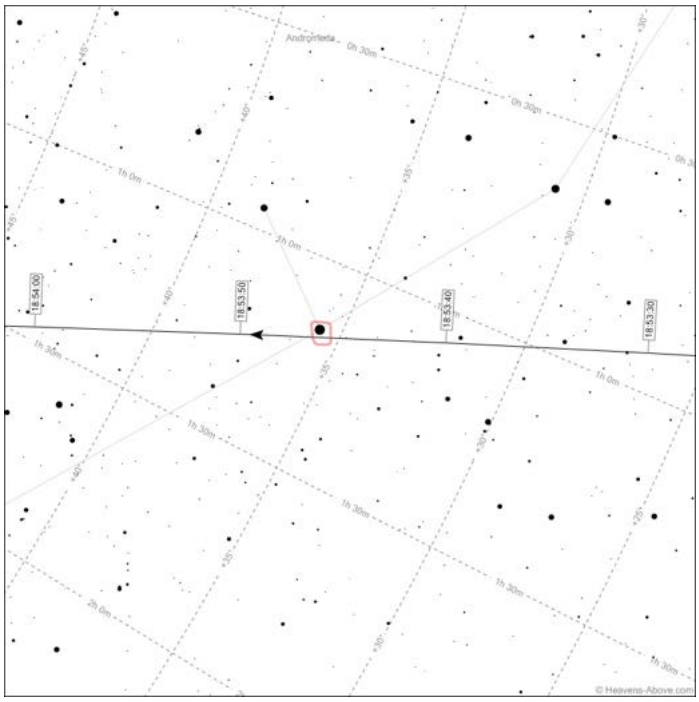

Figure 11. Heavens-Above.com image with estimated FOV of CZ-4 R/B observation

For the second observation, the Sich 1 satellite was recorded passing by a few stars close to the Cassiopeia constellation. Three stars were confirmed to be in view at the time of the satellite's passing. The recording was stopped just before the satellite fully exited the FOV as it was originally believed to have been missed and the recording was prematurely cancelled. Figure 12 below is a sky chart from Heavens-Above.com which depicts the object's predicted orbital path. Figure 13 below is zoomed in on the same sky chart with the approximate FOV of the recorded event outlined.

The third observation observed the Cosmos 2237 satellite. Even fewer stars were in view for this observation and no new information was gained that further improved research efforts.

The fourth observation captured the Starlink 1066 satellite as it passed between four stars close to the Perseus constellation. The telescope was shifted mid observation due to operator error which created a shift in the recorded satellite path.

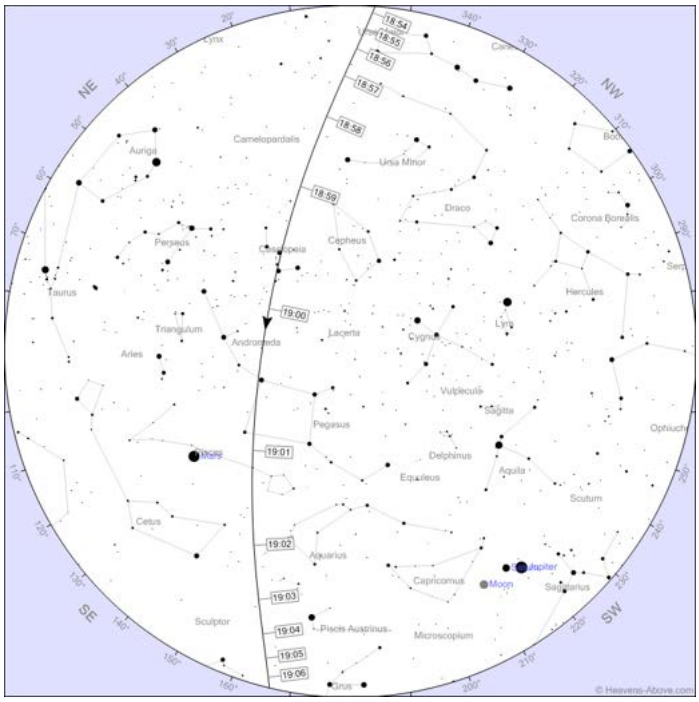

Figure 12. Heavens-Above.com image of CZ-4 R/B overhead pass

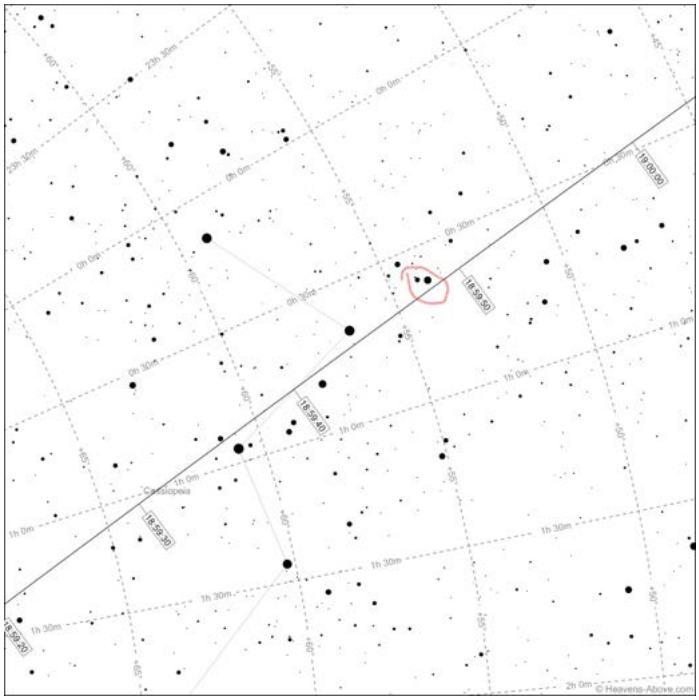

Figure 13. Heavens-Above.com image with estimated FOV of Sich 1 observation

Figure 14 below is a sky chart from Heavens-Above.com which depicts the object's predicted orbital path. Figure 15 below is zoomed in on the same sky chart with the

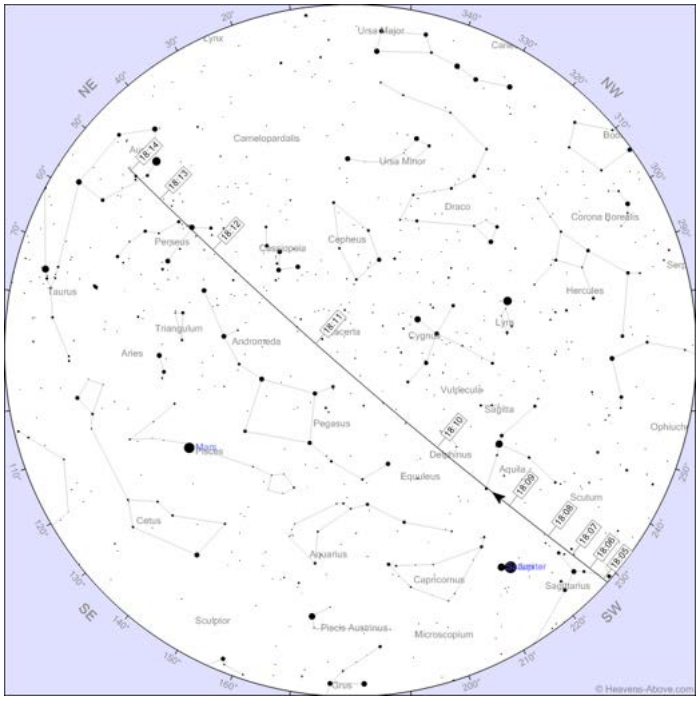

Figure 14. Heavens-Above.com image of Starlink overhead pass

approximate FOV of the recorded event outlined.

The fifth observation captured the Yaogan 1 satellite as it passed by five stars close to the Orion constellation. This observation caught the most stars in view, was undisturbed during the recording of the satellite path, and therefore had the best chance of being able to successfully provide the needed data to satisfy the research objectives. Figure 16 below is a sky chart from Heavens-Above.com which depicts the object's predicted orbital path. Figure 17 below is zoomed in on the same sky chart with the approximate FOV of the recorded event outlined.

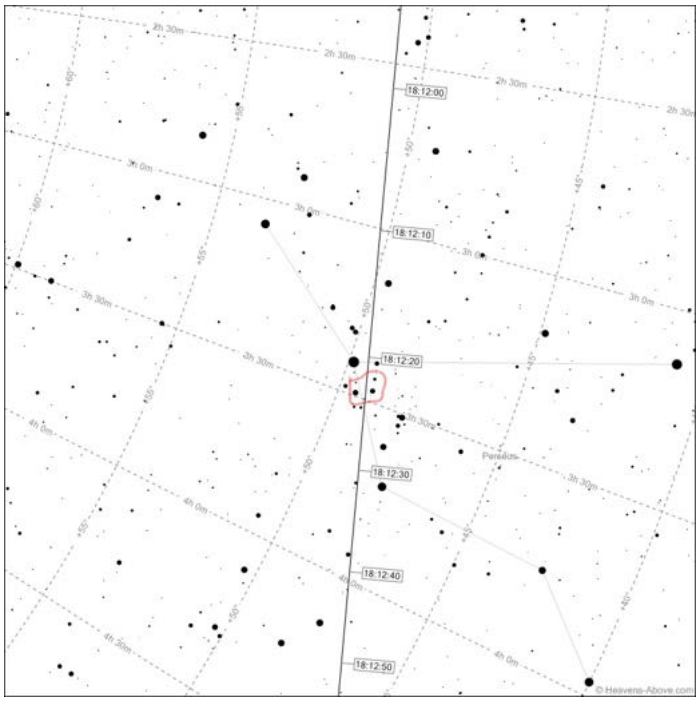

Figure 15. Heavens-Above.com image with estimated FOV of Starlink 1066 observation

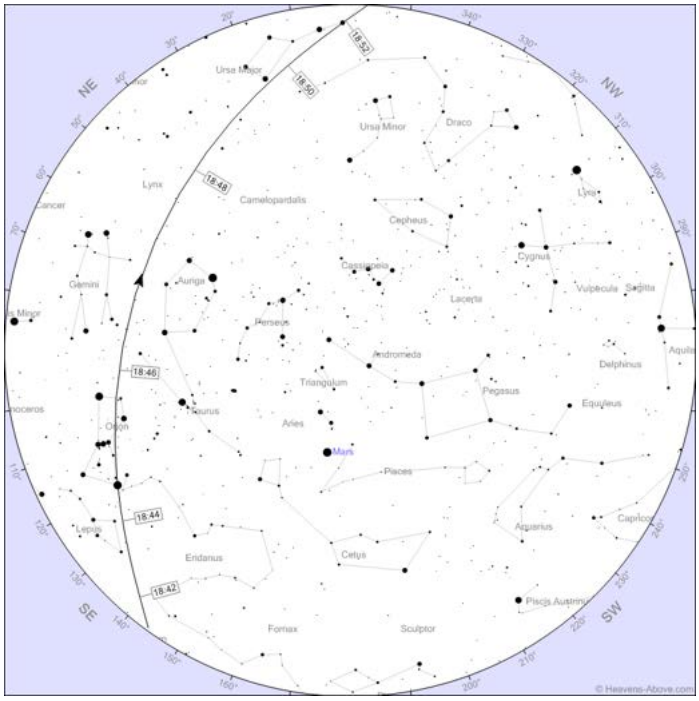

Figure 16. Heavens-Above.com image of Yaogan 1 overhead pass

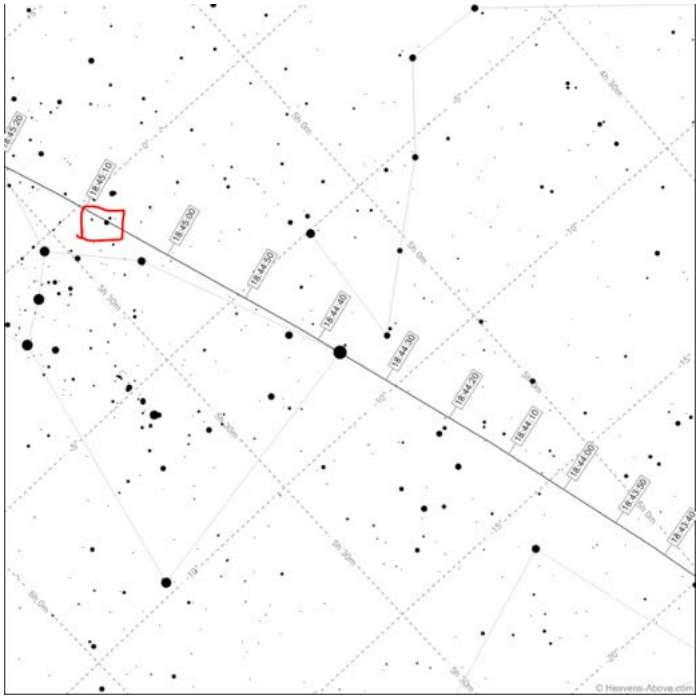

Figure 17. Heavens-Above.com image with estimated FOV of Yaogan 1 observation

3.1.4 Methodology for data analysis

Each observation file was imported into a python script where it was converted into four MATLAB ".m" files–one each for x and y pixel coordinates, one for polarity, and one for the event times. These files were then anaylzed in MATLAB. The approximate azimuth and elevation of the telescope was assigned as the center of the FOV for the camera's array. An estimated azimuth and elevation for each pixel was determined by using the width and height of the FOV and the number of pixels resulting in degrees per pixel for each dimension. The center azimuth and elevation for the observed object's orbit was estimated by manually determining the enter and exit angles within the FOV and calculating the center of the path captured in view.

TLE data for each observation was taken from space-track.com and initial position and velocity was created with Vallado's sgp4 code. An initial Gaussian covariance matrix was created and both were then rotated to the ECI reference frame using

direction cosine matrices. The telescope's position in ECEF frame was rotated to the ECI frame as well. Next the state of the object and covariance matrix was propogated from the TLE time to the observation time using two-body problem mechanics. Equations 7 and 8 are the equations used for the propogation.

$$\frac{dm}{dt} = \begin{bmatrix} dx & dy & dz \\ -\frac{\mu * x}{r^3} & -\frac{\mu * y}{r^3} & -\frac{\mu * z}{r^3} \end{bmatrix} \tag{7}$$

$\frac{dm}{dt}$ is the time rate for the state, μ is the gravitational parameter, r is the range vector for the object in the ECI frame, dx, dy, dz represent the velocity in the respective directions.

$$\frac{dP}{dt} = F * P + P * F' + M * Qs * M' \tag{8}$$

$\frac{dP}{dt}$ is the time rate for the covariance matrix, F is the dynamic Jacobian, P is the covariance matrix, M and Qs are terms that add in uncertainty from process and measurement noise.

Next, the range vector from the telescope to the object was calculated by subtracting the position vectors in the ECI frame and then converted to the topocentric frame in order to compare the telescope measurement to the expected measurement and eventually update the object's orbit to create a more accurate expected measurement. The initial guess for the expected azimuth, β_i and elevation h_i for the object is determined by Equations 9 and 10

$$\beta_i = \tan^{-1}\left(\frac{\rho_y}{\rho_z}\right) \tag{9}$$

$$h_i = \sin^{-1}(\rho_z) \tag{10}$$

For this research, the Kalman filter method updates the original orbit estimate

in order to account for some of the uncertainty previously mentioned in Chapter II. The measurement of the telescope's latitude and longitude, acquired from Google Maps, and the Meade mount's azimuth and elevation is brought in with the expected measurement and run through the Kalman update equations to generate an updated state and covariance. The Kalman filter update equation is shown for the covariance update in Equation 11 and state update in Equation 12

$$P(+) = P(-) - CK^T - KC^T + KWK^T \tag{11}$$

$$\delta x(+) = \delta x(-) + K(Z_{cam} - Z_{exp}) \tag{12}$$

$P(+)$ is the updated covariance matrix, $P(-)$ is the previous covariance, C is the cross covariance, K is the Kalman Gain and W is the innovations covariance which are calculated below in Equations 13, 15, and 14 respectively. $\delta x(+)$ is the updated ojbect state, $\delta(-)$ is the previous state, $Zcam$ is the measured azimuth and elevation angles, and $Zexp$ is the expected azimuth and elevation angles.

$$C = P(-)H^T \tag{13}$$

$$W = HP(-)H^T + R_k \tag{14}$$

$$K = CW^{-1} \tag{15}$$

H is the Jacobian matrix evaluated at the previous state $\delta_x(-)$ and R_k is a term that accounts for sensor imperfections. Equations 16 and 17 are needed to calculate the observation matrix.

$$\beta = \tan^{-1}\left(\frac{\rho_x \sin\theta - \rho_y \cos\theta}{\rho_x \cos\theta \sin\theta + \rho_y \sin\theta \sin\phi - \rho_z \cos\theta}\right) \tag{16}$$

$$h = \sin^{-1}(\frac{\rho_x \cos\theta\cos\phi + \rho_y \sin\theta\cos\phi + \rho_z \sin\phi}{\sqrt{\rho_x^2 + \rho_y^2 + \rho_z^2}}) \tag{17}$$

β and h are the angles for azimuth and elevation shown in Figure 5. θ and ϕ are the telescope's local mean sidereal time and latitude respectively. ρ and its subcomponents is the range from the telescope to the object.

Taking the partial derivatives of Equations 16 and 17 generates the components of the Jacobian matrix.

$$\frac{\delta\beta}{\delta x} = \frac{\rho_y \sin\phi - \rho_z \sin\theta\cos\phi}{(\rho_x \cos\theta\sin\phi + \rho_y \sin\theta\sin\phi - \rho_z\cos\phi)^2(\rho_x\sin\theta - \rho_y\cos\theta)^2} \tag{18}$$

$$\frac{\delta\beta}{\delta y} = \frac{\rho_z \cos\theta\cos\phi - \rho_x \sin\phi}{(\rho_x \cos\theta\sin\phi + \rho_y \sin\theta\sin\phi - \rho_z\cos\phi)^2(\rho_x\sin\theta - \rho_y\cos\theta)^2} \tag{19}$$

$$\frac{\delta\beta}{\delta z} = \frac{\rho_x \sin\theta\cos\phi - \rho_y \cos\theta\cos\phi}{(\rho_x \cos\theta\sin\phi + \rho_y \sin\theta\sin\phi - \rho_z\cos\phi)^2(\rho_x\sin\theta - \rho_y\cos\theta)^2} \tag{20}$$

$$\frac{\delta h}{\delta x} = \frac{(\rho_y^2 + \rho_z^2)\cos\theta\cos\phi - (\rho_x\rho_y \sin\theta\cos\phi + \rho_x\rho_z\sin\phi)}{\rho^2\sqrt{\rho^2 - (\rho_x\cos\theta\cos\phi + \rho_y\sin\theta\cos\phi + \rho_z\sin\phi)^2}} \tag{21}$$

$$\frac{\delta h}{\delta y} = \frac{(\rho_x^2 + \rho_z^2)\sin\theta\cos\phi - (\rho_x\rho_y \cos\theta\cos\phi + \rho_y\rho_z\sin\phi)}{\rho^2\sqrt{\rho^2 - (\rho_x\cos\theta\cos\phi + \rho_y\sin\theta\cos\phi + \rho_z\sin\phi)^2}} \tag{22}$$

$$\frac{\delta h}{\delta z} = \frac{(\rho_y^2 + \rho_x^2)\sin\phi - (\rho_x\rho_z \cos\theta\cos\phi + \rho_y\rho_z\sin\theta\cos\phi)}{\rho^2\sqrt{\rho^2 - (\rho_x\cos\theta\cos\phi + \rho_y\sin\theta\cos\phi + \rho_z\sin\phi)^2}} \tag{23}$$

All of the components together form the Jacobian Matrix H in the following format:

$$H = \begin{bmatrix} \frac{\delta\beta}{\delta x} & \frac{\delta\beta}{\delta y} & \frac{\delta\beta}{\delta z} \\ \frac{\delta h}{\delta x} & \frac{\delta h}{\delta y} & \frac{\delta h}{\delta z} \end{bmatrix} \tag{24}$$

3.1.5 Methodology Summary

This chapter discussed the methodology and techniques used during research to observe satellites and collect data. First, the telescope setups were explained which

outlined the hardware used. Next, the observations recorded were detailed. Finally, the methodology for processing and analyzing the data was described where the approximate telescope azimuth and elevation is used via the Kalman filter update equations to update the objects predicted orbit. The next chapter analyzes the data collected to determine the effectiveness of the neuromorphic camera at performing orbit updates for SDA.

IV. Analysis

4.1 Analysis

4.1.1 Introduction

This chapter analyzes the observations made, the data collected during satellite passes, and the results from applying the methodology mentioned in Chapter III.

4.1.2 Astrometry

The fourth observation, Starlink1066, was the first instance where enough stars might have been captured to attempt to apply astrometry and determine the pointing center of the telescope. After converting the file type and analyzing in MATLAB, the output image Figure 18 was generated. Four stars were captured at the same

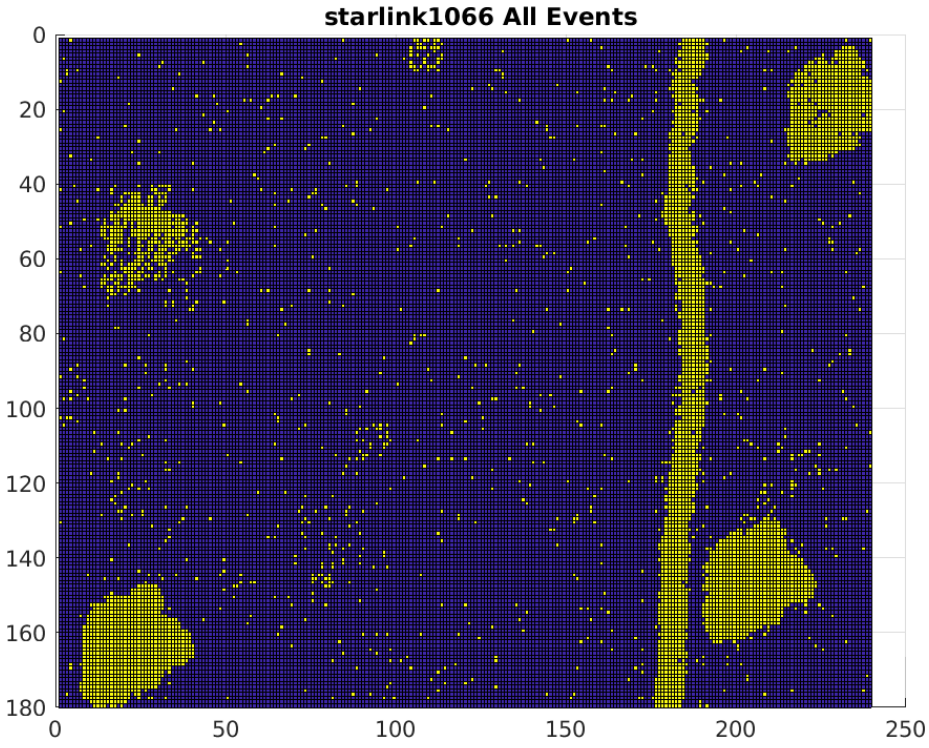

Figure 18. Observation 4 (Starlink 1066) Events

time as the object passing within the FOV. The generated image was run through astrometry.net in an effort to match the image to a star map but was unsuccessful. Figure 18 was posted to an astrometry.net help forum in an effort to seek help from someone more familiar with the code. The conversation resulted in determining that on average, astrometry.net needs 10-15 stars to be able to match an image to a star map.[24] After the discussion, focus was shifted from attempting to capture enough stars in view to apply astrometry towards finding a method to apply orbit updates with the data set already available.

4.1.3 Orbit Updates

Each observation was analyzed within MATLAB to generate an output image which depicts observed stars and the path of the object while attempting to reduce the amount of noise generated by the camera. The third observation was not processed due to having fewer stars than observation two and more noise. Figures 19, 20, 21, and 22 are the output images for each observation: [Figure 19 was taken with the Meade-10 inch telescope which observed CZ4RB passing from the right to the left of the FOV with one star in view. The remaining observations were taken with the Takahashi 106mm telescope to increase the FOV. Figure 20 shows the recording of Sich 1 which moved from the bottom of the FOV to the right in a diagonal path with three stars in view. The recording was stopped before the object left the FOV because the user believed the object was missed and pressed the stop recording button just as the object entered the FOV. Figure 21 shows the recording of Starlink 1066 as it passed from the top of the FOV to the bottom with four stars in view. The curve in observed path was a result of bumping into the telescope causing a shift in pointing. The final observation, Figure 22 recorded Yaogan 1 travelling from the right to the top of the FOV with three stars in view.

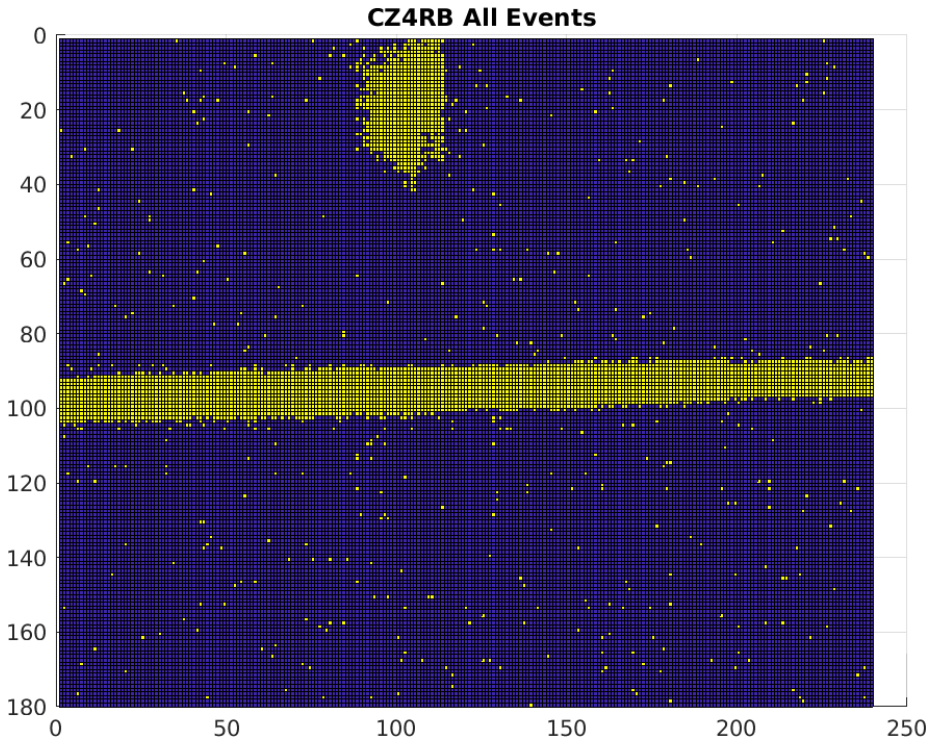

Figure 19. Observation 1 (CZ4RB) Events

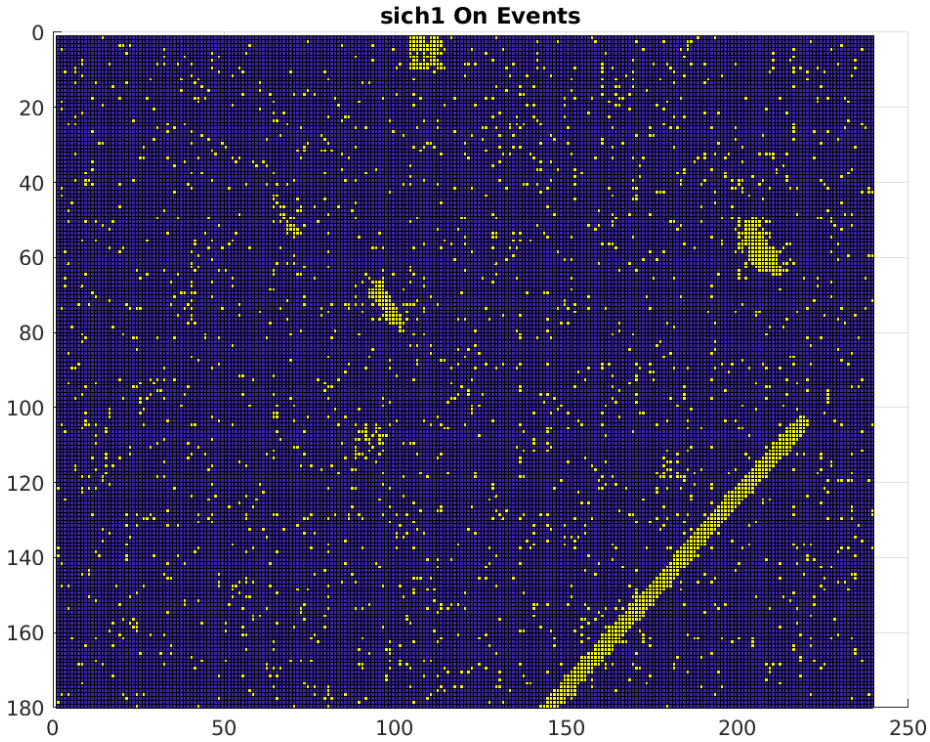

Figure 20. Observation 2 (Sich 1) Events

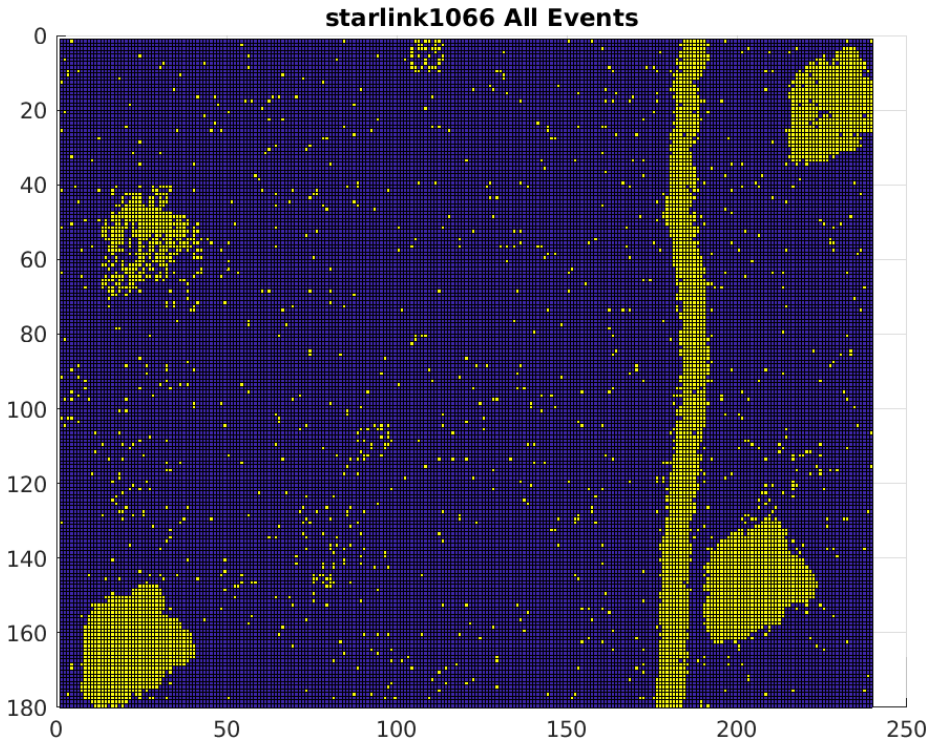

Figure 21. Observation 4 (Starlink 1066) Events

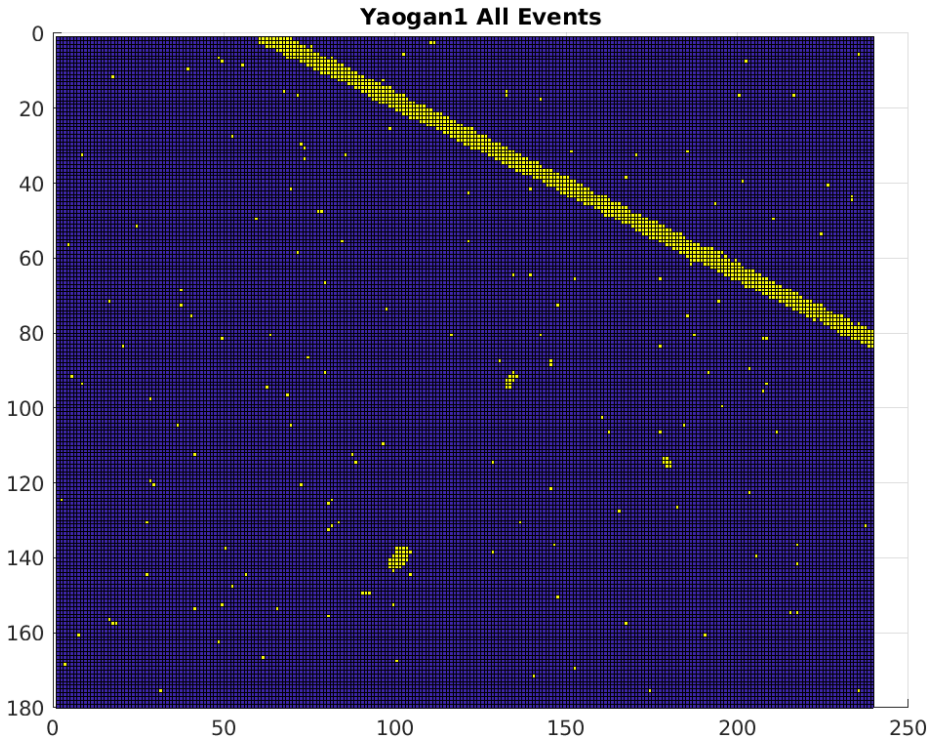

Figure 22. Observation 5 (Yaogan 1) Events

The midpoint of the objects observed path is approximated by taking the entry and exit pixel locations and dividing by two. This midpoint angles act as the observation within the Kalman filter update. Tables 3 and 4 compare the azimuths and elevations for the Meade telescope's measurement, the two-body propogated TLE state, and the updated propogated state.

Table 3. Starlink1066 Az/El Comparison

(Degrees)	Object	Propogated State	Updated Propogated State
Azimuth	58.23	62.51	62.26
Elevation	31.5	31.65	33.12
Distance from Object		4.28	4.34

Table 4. Yaogan1 Az/El Comparison

(Degrees)	Object	Propogated State	Updated Propogated State
Azimuth	303.11	304.95	318.39
Elevation	20.16	30.17	36.24
Distance from Object		10.17	22.18

A few known issues could have influenced the results. During observation 4, the telescope was shifted mid-recording which may have induced errors. For both observations 4 and 5, the lack of accuracy in pointing knowledge could also induce errors reducing effectiveness of the orbit update. Ideally, the output images for the observations should be processed through a tool like astrometry.net to accurately determine pointing knowledge but not enough stars were captured in the observations for the tool to function. Instead, the pointing knowledge was based upon the Meade 10-inch's telescope mount which contains built in azimuth and elevation measurements.

Perhaps most interesting about the data gathered from using the neuromorphic camera is that the timing of each event is also captured. Using the timing of the events, an idea of how quickly the angles change can be formed which is an additional type of data that cannot be acquired via ccd or cmos cameras. This would further improve the orbit update by adding more data to the Kalman filter. The equations

needed to incorporate the angle rates into the Kalman filter update can be derived by taking the partial derivatives of Equations 25 and 26.

$$\dot{\beta} = \frac{-x\dot{y}\sin\phi + x\dot{z}\cos\phi\sin\theta + y\dot{z}\cos\theta\cos\phi - z\dot{x}\cos\theta\cos\phi}{\left(x\cos\theta\sin\phi + y\sin\theta\sin\phi - z\cos\phi\right)^2 + \left(x\sin\theta - y\cos\theta\right)^2} \tag{25}$$

$$\dot{h} = \frac{\left(\dot{x}\cos\theta\cos\phi + \dot{y}\sin\theta\cos\phi + \dot{z}\sin\phi\right) - \dot{r}\left(x\cos\theta\cos\phi + y\sin\theta\cos\phi + z\sin\phi\right)}{r^2\sqrt{r^2 - \left(x\cos\theta\cos\phi + y\sin\theta\cos\phi + z\sin\phi\right)^2}} \tag{26}$$

4.2 Summary

Chapter IV discussed the results from applying the methodology to the research. First, the observations recorded were described. Next the data analysis was discussed, including the issues that could have produced the resulting error in angle estimation. The next chapter draws conclusions from the research conducted and discusses some potential next steps to further this research.

V. Conclusion

5.1 Conclusion

This section builds conclusions and answers the research questions originally posed based upon experimentation and data analysis. Then future research ideas are suggested which could further this endeavor.

Neuromorphic cameras pose an interesting technology that could be applied to and further efforts in SDA. While the results from data analysis resulted in some unexpected errors which could not be overcome, the fact remains that these cameras can potentially be used for SDA.

First, neuromorphic cameras can provide the same data relative to SDA as a CCD camera used in conjunction with a telescope. The azimuth and elevation angles can be determined for objects recorded in view by using the telescope's look angles as the center of the FOV and then deriving the amount that the azimuth and elevation changes with each pixel. These angles would be more accurate if a tool like astrometry.net were used to determine a more accurate pointing estimate. Perhaps a boresighted wide-FOV sensor could be used in addition to the setups utilized in this research to capture additional stars in view to allow the use of such tools. Since neuromorphic cameras also record timestamps for each event that occurs, the rate of change for the look angles can also be determined. Standard CCD cameras can provide change rate data by differencing frames but the methods outlined in Chapter IV should be more accurate.

Second, this research shows that based upon the data collected and techinques applied, it is possible to perform orbit updates for observed objects with a neuromorphic sensor. The look angles determined for the object's observed path were used as part of a Kalman filter update. Using TLE data, the state of the object was propa-

gated forward to the observation time via two-body problem methods. Observation data was also applied and used in a Kalman filter update to propagate the TLE data forward. Unfortunately, inaccurate pointing knowledge was used for the angle calculations since the telescope azimuth and elevation was measured by attempting to point two telescopes at the same location.

Finally, this research was unable to show that neuromorphic cameras can be used for astrometry purposes. This was not due to the unique operation of the cameras. Instead, the equipment setup and location used for recording observations was likely the cause. Not enough stars were ever visible during an object's passing to be able to determine the sensor's true pointing angles. If a different telescope was used that provided a wider FOV or had a wider aperture that could collect more light or if a better observation location was used that suffered from less light pollution, more stars would have been visible. Despite the apparent issues, it should be clear that neuromorphic cameras have the potential to provide a novel approach to improving SDA.

5.2 Future Research

Research in the field of neuromorphic cameras and their applicability to SDA is far from finished. Many potential avenues for further research and development exist, to include:

1. Resolving the underlying issues that resulted in the error in pointing estimate by applying the astronometric techniques mentioned in Chapter II.

2. Capturing more stars in view during an object's passing in order to apply astronometric techniques to further improve orbit update estimates by moving to a darker location or changing equipment setup to widen the FOV.

3. Incorporate the angle rate change calculations started in Chapter IV into the Kalman filter update to produce a more accurate orbit update by taking the partial derivatives of Equations 25 and 26 and concatenating the results to the Jacobian matrix.

Bibliography

1. T. Delbruck, "Neuromorphic vision sensing and processing," tech. rep., Inst. of Neuroinformatics, University of Zurich and ETH Zurich, 2016.

2. R. Benosman, S.-H. Ieng, C. Clercq, C. Bartolozzi, and M. Srinivasan, "Asynchronous frameless event-based optical flow," *Neural Networks*, vol. 27, no. 1, pp. 32–37, 2012.

3. Meade Instruments Corporation, "Types of telescopes." [Online; accessed 19-February-2021].

4. W. E. Wiesel, *Modern Orbit Determination*. Aphelion Press, 2003.

5. O. Montenbruck and T. Pfleger, *Astronomy on the Personal Computer*, ch. 12, pp. 251–266. Springer-Verlag Berlin Heidelberg, 2000.

6. M. J. Holzinger and M. K. Jah, "Challenges and potential in space domain awareness," *Journal of Guidance, Control, and Dynamics*, vol. 41, no. 1, p. 1, 2018.

7. NASA, "Satellite collision leaves significant debris clouds," *Orbital Debris Quarterly News*, vol. 13, no. 2, pp. 1–2, 2009.

8. M. R. Endsley, "Toward a theory of situation awareness in dynamic systems," *Human Factors*, vol. 37, no. 1, pp. 32–64, 1995.

9. P. Lichtsteiner, C. Posch, and T. Delbruck, "A 128× 128 120 db 15 μs latency asynchronous temporal contrast vision sensor," *IEEE Journal of Solid-State Circuits*, vol. 43, no. 2, pp. 566–576, 2008.

10. R. Benosman, C. Clercq, X. Lagorce, S.-H. Ieng, and C. Bartolozzi, "Event-based optical flow," *IEEE Transactions on Neural Networks and Learning Systems*, vol. 25, no. 2, pp. 407–417, 2013.

11. J. Boettiger, "A comparative evaluation of the detection and tracking capability between novel event-based and conventional frame-based sensors," Master's thesis, Air Force Institute of Technology, 2020.

12. G. Cohen, S. Afshar, and A. van Schaik, "Approaches for Astrometry using Event-Based Sensors," in *The Advanced Maui Optical and Space Surveillance Technologies Conference* (S. Ryan, ed.), p. 38, Sept. 2018.

13. D. A. Vallado, *Fundamentals of Astrodynamics and Applications (Third Ed.)*, pp. 87, 258, 265–272. Space Technology Library, 2007.

14. D. Lang, D. W. Hogg, K. Mierle, M. Blanton, and S. Roweis, "Blind astrometric calibration of arbitrary astronomical images," 2009.

15. C. Frueh, H. Fielder, and J. Herzog, "Heuristic and optimized sensor tasking observation strategies with exemplification for geosynchronous objects," *Journal of Guidance, Control, and Dynamics*, 2017.

16. A. Nafi and K. Fujimoto, "A Unified Approach for Optical Survey Strategies Design of Resident Space Objects," in *Proceeding of the AAS/AIAA Astrodynamics Specialist Conference*, Sept. 2016.

17. J. Ferreira, I. Hussein, J. Gerber, and R. Sivilli, "Optimal SSN Tasking to Enhance Real-Time Space Situational Awareness," in *Proceeding of the AMOS Technical Conference*, Sept. 2016.

18. M. Schmunk, "Initial determination of low earth orbits using commercial telescopes," Master's thesis, Air Force Institute of Technology, 2008.

19. J. McCafferty, "Development of a modularized software architecture to enhance ssa with cots telescopes," Master's thesis, Air Force Institute of Technology, 2016.

20. Takahashi Seisakusho Ltd., *Flat-Field Super Quadruplet FSQ-106ED Instruction Manual*.

21. Meade Instruments Corporation, *Instruction Manual 8", 10", 12", 14", 16" LX200-ACF Advanced Coma-Free Telescopes with GPS and AutoStar II Hand Controller*, 2009.

22. Chris Peat, "Heavens-above.com." [Online; accessed 22-February-2021].

23. Inivation, "dvs240 user manual." [Online; accessed 22-February-2021].

24. J. Bacon and Dustin, "Astrometry.net and neuromorphic camera data," 2020. [Online; accessed 7-Dec-2020].